# Photo-activated thin films of porphyrins for reactive oxygen species generation

**Dáire J. Gibbons,[a, b] Alexandre Boh,[c] Benoit Habermeyer,[c] Nicolas Villandier,[a] Stéphanie Leroy-Lhez*[a]** and **René M. Williams*[b]**

[a] *PEIRENE – EA7500, Faculty of Sciences and Technology – University of Limoges, 123 avenue Albert Thomas, 87060 Limoges, France.*

[b] *Molecular Photonics Group, Van't Hoff Institute for Molecular Sciences (HIMS), Universiteit van Amsterdam, Science Park 904, 1098 XH Amsterdam, Netherlands.*

[c] *PorphyChem SAS, 9 Avenue Alain Savary, 21000 Dijon, France.*

*Received date (to be automatically inserted after your manuscript is submitted)*

*Accepted date (to be automatically inserted after your manuscript is accepted)*

**ABSTRACT:** The use of a single component porphyrin thin-film for photodynamic antimicrobial chemotherapy is unexplored. Herein, a porphyrin with good film formation properties is used to make thin layers, by physical vapor phase deposition, that are stable in aqueous media and can generate singlet oxygen upon 650 nm excitation. The synthesis and photophysical studies, in solution and as thin film, of free base 5,10,15,20-tetra-(4-hexyloxyphenyl)-porphyrin are described. The porphyrin was synthesized *via* modified Adler-Longo conditions. Thin films of this porphyrin were made on quartz glass *via* spin coating and *via* vapour-phase deposition. The porphyrin was studied, in solution and as thin film (without a polymer component or matrix), with UV-Vis spectroscopy and with steady-state and time-resolved photoluminescence spectroscopy. The spin coated films display sharp J-band emission at 741 nm, indicating J-aggregate formation, but are not stable in aqueous media. The thin films obtained *via* vapour-phase deposition do not show the J-band emission, but are stable. The detection of singlet oxygen generated by the porphyrin thin film using a chemiluminescent water-soluble singlet oxygen probe is reported.

**KEYWORDS:** Photodynamic therapy, Photo Antimicrobial ChemoTherapy, THOPP, Photophysical characterization, Solution, Solid thin film, Aquaspark, Singlet oxygen

***Correspondence** to Dr. René M. Williams, Tel: + 31 (0)20 525 5477, Fax: + 31 (0)20 525 6456, Email: r.m.williams@uva.nl and Dr. Stéphanie Leroy-Lhez, stephanie.lhez@unilim.fr

## INTRODUCTION

The first written accounts of Photodynamic Therapy (PDT) were made at the end of the 19th century [1]. Back then, it was named 'phototherapy' [2] and has since been developed to treat early stage tumours [3], dermatological conditions [4] and microbial infections (Antimicrobial Photodynamic Therapy, APDT) [5]. More recently, PDT has been shown to act as a priming and optical imaging tool [6]. Interestingly, photodynamic priming refers to the fact that PDT leaves a type of physiological marker. This occurs by a transient change of the host's microenvironment, thus making the target more receptive to subsequent additional therapies, like chemo- and immuno-therapy.

PDT requires the presence of molecular oxygen ($^3O_2$), a photosensitizer (PS) and light to form singlet oxygen ($^1O_2$), and reactive oxygen species, that are responsible for the desired therapeutic effect [7]. The 'ideal PS' is highly desired and its properties are extensively described in reviews by Callaghan and Senge, and by Abrahamse and Hamblin [1, 8]. Some of these properties include efficient triplet excited state formation with an excitation wavelength in the 650–850 nm region (known as the therapeutic window) [9], possessing a sufficiently long triplet lifetime [10], and generating high yields of singlet oxygen and Reactive Oxygen Species (ROS) [11]. The inclusion of metals and heavy (halogen) atoms are a common method to increase the singlet oxygen and ROS production, as well as the triplet yield, *via* the so-called heavy-atom effect. However, these heavy atoms come with their drawbacks that include increasing the cost, elevated dark toxicity and poor photostability [12, 13]. Following irradiation of a PS, the singlet state is populated. This singlet state can then undergo intersystem crossing (ISC) to form the triplet state, which can interact with $^3O_2$ to form $^1O_2$ (Fig. **1**), which is capable of destroying cancer cells or microbial cells [14].

<Fig. **1**>

Antimicrobial Photodynamic Therapy (APDT) is the light-treatment against harmful micro-organisms and has been applied in the clinics for almost thirty years [15]. It is used to treat infections [16], oral infections in dentistry [17] and more recently, it has been investigated as an alternative pest management in agriculture [18]. In order to treat microbial infections in the clinic, photosensitizers have to be physically applied to the surface of the infected areas. Furthermore, PSs have been incorporated into thin films for their use as photodetectors and sensors [19, 20].

The PS used in this study is 5,10,15,20-tetra-(4-hexyloxyphenyl)porphyrin (**THOPP**), that was synthesized for the first time in 1993 by Shimizu *et al* [21]. The authors described the mesomorphic phase transitions of *meso*-tetra-(4-alkoxyphenyl)porphyrins with different chain lengths. Furthermore, it has recently been shown that the Zn(II) complex of **THOPP** can display electro-luminescence in thin film devices [22]. **THOPP** has also appeared in papers that report on volumetric properties of porphyrins [23], oxygen sensing [24], fluorescence and FTIR analysis [25], mesogenic properties of porphyrin liquid crystals [26] and organic-inorganic surfaces in thin films [27].

Since *meso*-tetra-(4-alkoxyphenyl)porphyrins can form well-ordered films that exhibit luminescence and as a molecular species can sensitize oxygen and act as photosensitizers [22, 24], **THOPP** was selected in order to investigate the possibility of creating singlet oxygen, *via* light excitation, with thin films. The good film formation properties were especially important in the selection of this porphyrin for our work. Herein, the synthesis of *meso*-tetra-(4-hexyloxyphenyl)porphyrin, **THOPP**, and its photophysical properties in solution, as well as in thin films, are described for application in photomedicine.

## RESULTS AND DISUCSSION

### SYNTHESIS

The synthesis of **THOPP** was conducted using modified Adler-Longo porphyrin condensation conditions (see Fig. 2) in a 12% yield [28]. This yield is slightly lower than reported in literature (16% yield) and the reason for this slight reduction in yield is likely due to the increase in the scale of the reaction (5 g aldehyde starting material used versus 2 g in literature) [22].

<Fig. **2**>

**THOPP** was characterized using $^{1}H$ and $^{13}C$ NMR spectroscopy, mass spectrometry, UV-Vis spectroscopy and normal-phase HPLC (Figs **S1**–**S6)**. The $^{1}H$ NMR spectrum (Fig. **S1**) indicates the formation of the desired porphyrin, in agreement with literature data [22]. The $^{13}C$ NMR spectrum (Fig. **S2**) clearly shows the hexyloxy tail and five aromatic resonances. Due to the fast exchange of the two NH protons in the tetrapyrrole ring (tautomerism), the α and β carbons of the pyrrole units coalesce into one broad peak at ~132 ppm. These effects have been described for porphyrins already in 1975 [29], and have also been reported for **THOPP** more recently [22].

The MALDI TOF mass spectrum of **THOPP** (Fig. **S3**) shows two main peaks at 1015 $(M+H)^+$ and 226 (dithranol matrix). In fig. **S4**, the $(M+H)^+$ peak is the most intense, similar to the mass spectrum of **TPP** [30]. Furthermore, protonated species of porphyrins in mass spectra are well known [31, 32]. The protonation is expected due to the acidic matrix. The molecular ion peak shows the expected isotope pattern (see fig. **S4**).

The HPLC analysis shows that there are no coloured impurities in the product (Fig. **S5**). The product in $CHCl_3$ was analysed with HPLC (normal phase column; stationary phase = $SiO_2$ and mobile phase = $CHCl_3$). The elution time of the product was 2.94 minutes with detection at 420 nm. No other products or impurities were detected during the HPLC analysis indicating a purity of >99%, assuming a single component peak. The peak experiences a slight tailing effect, which is typical for porphyrin samples analysed using HPLC [33], especially with a normal phase column. There were no other peaks detected apart from the one shown in fig. **S5**. The melting point (274.9 -> 275.6 ºC) was slightly higher than reported earlier (271 ºC) [21]. The UV-Vis spectrum of **THOPP** in THF is included in Fig. **S6**. It shows a characteristic porphyrin UV-Vis absorption spectrum (see below for discussion).

### PHOTOPHYSICAL CHARACTERIZATION

The photophysical properties of **THOPP** were studied in solution and as a thin film. Results are summarized into tables **1**–**4** and commercially available 5,10,15,20-tetraphenylporphyrin (**TPP**) was used as a reference for properties in solution (see structure of **TPP** in fig. **2**).

### SOLUTION PROPERTIES

UV-Vis spectra of **THOPP** and **TPP** in chloroform ($CHCl_3$) or THF as solvent are characteristic of free base porphyrins with an intense Soret band at 423 nm and 418 nm, respectively (Table **1**) [34]. These Soret bands both bear shoulders with maxima at 400 nm and four Q-bands are observed (Q-band maxima are summarized in Table **1**). [35]. **THOPP** was also studied in tetrahydrofuran (THF; see UV-Vis spectrum in fig. **S6**), a very good solvent for **THOPP**. Upon changing the solvent from $CHCl_3$ to THF, the Soret band shifts towards the blue region by 2 nm (Table **1**). The Q-bands absorbed less light (as indicated by their reduced molar absorption coefficients), and they shifted to the blue region by a max of 3 nm.

**THOPP** undergoes a bathochromic shift (4–9 nm) of all bands, compared to **TPP**. This is most likely due to the presence of electron-donating hexyloxy chains on the *para*-position of the phenyl rings. This structural difference therefore causes a shift towards the red region of the UV-Vis spectrum. The photoluminescence spectra were recorded in tetrahydrofuran (THF) and $CHCl_3$ to determine the fluorescence quantum yield ($\Phi_f$) and the singlet oxygen quantum yield ($\Phi_\Delta$), respectively. Fig. **S11** shows the determination of the energy of the first excited state, $S_1$, of **THOPP** and **TPP** in $CHCl_3$.

**THOPP** shows a Soret band that absorbs slightly less than **TPP** as shown by its lower molar absorption coefficient (Table **1**). However, the Q-bands of **THOPP** absorb more and their intensity ratio is different compared to **TPP** in $CHCl_3$. The intensity of these bands of **THOPP** in decreasing order, from longer to shorter wavelengths (low energy to high energy), are: $Q_{IV} > Q_{III} > Q_I > Q_{II}$. In **TPP**'s UV-Vis spectrum, the Q-bands decrease in order of: $Q_{IV} > Q_{III} > Q_{II} > Q_I$, with the $Q_{IV}$-peak much more intense than the others. This intense peak is followed by minor decreases in intensity from the $Q_{III}$ to $Q_I$ in the UV-Vis spectrum of **TPP**. However, **THOPP** shows a gradual decrease from $Q_{IV}$ to $Q_{III}$, followed by a large decrease to the $Q_{II}$. Surprisingly, the intensity almost doubles from the $Q_{II}$ to $Q_I$ in the UV-Vis spectrum of **THOPP**. These differences in the intensity ratio and position of the Q-bands are accredited to the molecular structure, influencing the frontier molecular orbital scheme. Previous reports of **THOPP** show identical UV-Vis spectra [22, 24, 25, 27].

<Table **1**>

The emission spectra of **THOPP** and **TPP** in $CHCl_3$ at room temperature are shown in fig. **S7**. The fluorescence quantum yield ($\Phi_f$) obtained for **THOPP** in $CHCl_3$ was 0.22 and it was determined using **TPP** in toluene as a reference ($\Phi_f = 0.11$) [36]. The emission maxima of **THOPP** appear at 655 nm and 725 nm. The former (Em1 as shown in Table **2**) is approximately three times more intense than the latter emission maximum (Em2). The fluorescence of **THOPP** in THF was also recorded (Fig. **8**). The position of the emission maxima, and the overall emission shape, remain unchanged upon changing the solvent from $CHCl_3$ to THF. Furthermore, the $\Phi_f$ of **THOPP** in both solvents remains unchanged (Table **2**).

**TPP** exhibits emission maxima at 649 nm and 718 nm in $CHCl_3$ (Fig. **S7**). All solutions (**TPP** in $CHCl_3$, and **THOPP** in $CHCl_3$ and THF) were excited at 518 nm and the absorbance at this wavelength was 0.1. **TPP**'s emission spectrum conforms to literature and appears to have a more bimodal distribution shape as the Em1 emission band is almost 1.6 times more intense than the Em2 peak [37]. **TPP**'s emission is overall less intense than that of **THOPP**. The $\Phi_f$ (**THOPP**) in this report is larger than previously reported (0.22 vs 0.13) by Şen *et al*. [25]. This difference is likely due to the different reference used for calculating the $\Phi_f$ by Şen *et al*. In their article, they used coumarin-153 in methanol as the reference [38]. Furthermore, the $\tau_s$ reported herein (9 ns) is twice as long compared to that reported by Şen and co-workers (~ 4.5 ns). The fluorescence of **THOPP** in $CHCl_3$ is displayed in Fig. **S7,** the quantum yield ($\Phi_f$) is 0.22. The fluorescence of **TPP** is lower than that of **THOPP** (Table **2**). This is in agreement with the results of Topal et al. [24] who reported $\Phi_f = 0.18$ for **THOPP** in toluene solvent.

<Table **2**>

The overlap of the absorption and emission spectra for **THOPP** and **TPP** in $CHCl_3$ determines the experimental energy of the singlet excited state ($E(S_1)$; Fig. **S9**). The $E(S_1)$ of **THOPP** is 654 nm (1.90 eV) and 648 nm (1.91 eV) for **TPP**. The energy of the $S_1$ ($E(S_1)$) is slightly lower for **THOPP** than for **TPP** and thus explains the

bathochromic shift observed in the UV-Vis spectrum of **THOPP**, compared to **TPP**. This $S_1$ energy level of **THOPP** and **TPP** is in close agreement with the literature value of 646 nm (1.92 eV) of **TPP** [39].The $\Phi_\Delta$ of **THOPP** in $CHCl_3$ was calculated using **TPP** in $CHCl_3$ as a reference ($\Phi_\Delta = 0.55$; Fig. **3**) [40]. The higher $\Phi_f$ in **THOPP** (Table **2**) and the decreased singlet oxygen quantum yield of **THOPP** (0.44) indicates that intersystem crossing (ISC) in **TPP** is likely faster than in **THOPP**.

<Fig. **3**>

In fig. **4**, the nanosecond transient absorption spectroscopy of **THOPP** in aerated THF is reported. The experiment was first conducted in $CHCl_3$, however the sample decomposed after excitation by the pump laser (see experimental details). There was no decomposition observed in THF and the decay curve of this aerated sample is fitted mono-exponentially (Fig. **4**). The oxygen-free sample of **THOPP** in THF decays bi-exponentially (Table **2** and fig. **S10**). This indicates that triplet-triplet annihilation is predominantly occurring and this decay channel undergoes second order decay kinetics. There is a slow and fast component observed and the slow component likely corresponds to the intrinsic lifetime of the triplet excited state of **THOPP** in oxygen-free THF (Fig. **S10**). The fast component would then correspond to triplet-triplet annihilation occurring (Table **2**). The lifetime of TPP in DMF was reported to be slightly longer than that of **THOPP** in THF (Table **2**) [41].

<Fig. **4**>

Table **2** reports a bi-exponential fit of the triplet decay data, however, a more appropriate model is second order decay kinetics. The observed triplet lifetime ($\tau_T$) is influenced by the triplet state being quenched by oxygen in solution, as well as by triplet-triplet annihilation ($k_{TT}$), and by the intrinsic triplet decay ($k_0$). Within the triplet-triplet annihilation process, the diffusion rate of the molecules in the triplet excited state, as well as their concentration at time zero ($C_0$; influenced by laser-power), play an important role due to bimolecular collisional quenching [42, 43].

The complex decay of triplet states and their interaction with oxygen also implies that singlet oxygen emission is due to a process with second order kinetics. This means that it can be fitted *via* a bi-exponential decay, as the concentration of the triplet at time 0 ($C_0$ in equations **1-3** below) and the concentration of oxygen in solution, are of importance. The triplet decay can be fitted by a mono-exponential function if the interaction with oxygen is fast. Furthermore, it is clear that the total removal of oxygen is not straightforward, indicated also by the fact that the singlet oxygen emission intensity remained unchanged upon prolonged bubbling with argon. These effects have also been noted by others [43].

By using second order decay kinetics at room temperature in THF, we obtain an intrinsic triplet lifetime of $\tau^0_T$ = 566 µs, and a triplet-triplet annihilation rate constant of $k_{TT} = 9.1 \times 10^9$ $M^{-1}.s^{-1}$. This is close to the diffusion rate in THF, which is $1.3 \times 10^{10}$ at 293 K. For pristine $C_{60}$ in toluene [44] at room temperature, $\tau^0_T \geq 280$ µs, with a $k_{TT} \geq 4.8 \times 10^9$ $M^{-1}.s^{-1}$ was reported. The intrinsic triplet state lifetime $\tau^0_T$ of TPP is reported to be 1500 µs at 293 K [39]. This implies that the values reported here are within the range of expectation.

The (partly spectrally integrated) data vs time ($t$) was fitted with a home-made Igor procedure describing the following function (Equations **1-3**):

$$\Delta A(t) = \frac{C_0 k_0}{k_0 e^{(k_0 t)} + k_{TT} C_0 (e^{(k_0 t)} - 1)}$$ (Equation **1**)

Perhaps superfluous to note, this is mathematically equivalent to

$$\Delta A(t) = \frac{C_0 e^{-(k_0 t)}}{1 + C_0 (k_{TT}/k_0)(1 - e^{(k_0 t)})}$$ (Equation **2**)

as well as

$$\Delta A(t) = \frac{C_0 k_0}{e^{(k_0 t)}(C_0 k_{TT} + k_0) - C_0 k_{TT}}$$ (Equation **3**)

as used by others [42, 43].

The concentration of the triplet excited state at time zero ($C_0$) was estimated by using the absorbance of the sample, the starting concentration, the excited volume (and depth), as well as the number of photons per pulse and was estimated to be $3.26 \times 10^{-6}$ M. Based on the molar absorption coefficient of the triplet state of TPP at 790 nm of 6000 $M^{-1}.cm^{-1}$, a concentration of triplet excited state at time zero ($C_0$) of $8.3 \times 10^{-6}$ M was estimated. It has to be noted that the exact outcome of the fitting procedure is rather sensitive to the $C_0$ value, but within reasonable limits of the $C_0$ value (between 10% and an absolute maximum of 100% of the ground state concentration, $3.26 \times 10^{-5}$ M). The variation of the outcome (of $k_{TT}$) is then a factor of ten.

Interestingly, and quite surprisingly, it has been reported that THF can react with singlet oxygen to form THF-singlet oxygen adducts [45]. Therefore, it is possible that the THF solvent slightly affects the triplet lifetime obtained. However, the reaction conditions reported by Sagadevan *et al*. show that these adducts are unlikely to form in our TA measurements. In particular, this paper reported reaction conditions of 2 hours irradiation with a blue LED light source (460 nm, 40 $mW/cm^2$). Our experiments were only 40 minutes in length with a pulsed laser (517 nm, 9 mW), which is too short for THF-singlet oxygen adduct formation.

The singlet excited state of **THOPP** decays mono-exponentially in THF (Fig. **S11**). This $S_1$ lifetime is 9.33 ns and is almost 6 times longer than the Zn(II) derivative of this compound (1.51 ns in THF) [22]. However, the free base of **THOPP** in THF has a slightly shorter $S_1$ lifetime than **TPP** in DMF (10.6 ns) [41].

**Solid film properties**

**THOPP** was dissolved in THF (10 mg $mL^{-1}$) and spin coated to make thin films on quartz glass. The UV-Vis spectrum was recorded and compared to **THOPP** in THF solution (Fig. **5**). The data is summarized in Table **3**.

**Film UV-Vis spectra**

Some differences were observed between the UV-Vis spectra of **THOPP** in solution and in the film. The major difference observed in the thin film spectrum (Fig. **5**) is a large 19 nm red-shift of the Soret band in the thin film (Table **3**). As previously reported by Magna et al. [46], this large shift in the absorption maxima is the first indication of the presence of (J)-aggregates in the thin film. Other small deviations between the UV-Vis of **THOPP** in the film and in solution, are seen in the positions of the Q-bands, with the largest difference observed in the $Q_{II}$ band (hypsochromic shift of 5 nm). In terms of Q-band characteristics, those of **THOPP** in the film are approximately the same width as in

solution (approximately 40 nm for $Q_{IV}$). Furthermore, there is a higher $Q_{III}$ to Soret band ratio in the film compared to solution ($Q_{III}$ / Soret = 0.12 vs 0.02; Fig **5**).

Compared to the **Zn(II)THOPP** (2 Q-bands) in a thin film [22], the free base **THOPP** thin film contains four Q-bands in the porphyrin film due to the absence of a metal in the core, which is known to occur because of symmetry [47]. The Soret band in the Zn(II) species is slightly blue-shifted (438 nm) compared to the free-base counterparts (440 nm), with the Q-bands of the Zn(II) species appearing at 560 nm and 602 nm [22].

<Fig. **5**>

<Table **3**>

**Emission spectra of films**

The excitation wavelength used for the emission spectrum of the **THOPP** thin film is 440 nm and the porphyrin emission is visible in the 600–800 nm region (as seen in fig. **6**). Interestingly, there is a sharp emission peak that arises at 741 nm which does not appear in the emission spectrum of **THOPP** in THF nor in $CHCl_3$ solution (Fig. **S7 + S8**). This peak, in the emission spectrum of the **THOPP** film, most likely appears due to the presence of J-aggregates in the film [48-50]. The presence of aromatic groups at the *meso* positions in porphyrins has been reported to enhance the formation of J-aggregates [51, 52]. The peak presence, at 741 nm, can be influenced by making thin films *via* physical vapour-phase deposition (PVD, see fig. **9**). Whereas the **THOPP** molecules in these PVD films can only interact with each other and (thus can be considered aggregated) they are not well organized. It is important to note that J-aggregates, characterized by the sharp J-band emission, are well ordered stacks of molecules, that are aligned. The J-band is generally more intense than the Em2 peak. There is almost no Stokes shift in the film compared to the solution and this differs in the Zn(II) species [22], where there is the presence of a larger Stokes shift. In a clear **THOPP** solution, the emission spectrum is indicative of a monomeric molecular species. Whereas in the **THOPP** spin coated film, the sharp peak (741 nm) in the emission spectrum of this film, suggests that the porphyrin forms J-aggregates in the film.

<Table **4**>

Fig. **6** shows the emission spectrum of **THOPP** in solution and on a quartz film that was obtained *via* spin coating. As discussed above, the emission is similar to that observed in solution, however there is a large peak at 741 nm that is due to the formation of J-aggregates in the thin film (see below).

<Fig. **6**>

**Porphyrin aggregation: J-band emission**

The sharp features of the new emission band (at 741 nm) in the films are reminiscent of J-band emission [51]. A useful description of J-aggregates is provided by Dong et al. [49]. There it is clarified that "whereas theoretically two molecules can make up a J-aggregate, the well-defined excitonic states in J-type dimers, trimers, tetramers up to decamers can be named more precise. We can assume that typical J-aggregate properties arise above 10 (up to 50) monomers. In general, the typical J-band, attributed to directional orientation of the transition dipoles of the molecules in the aggregate, starts to be clearly observed when N is larger than 50. The minimum number of monomers that is needed to form a typical J-

aggregate is related to the exciton (diffusion) length. The aggregate length should be as long as the exciton (diffusion) length, which will be influenced by the molecular (monomer) structure. Up to a certain length however, some photophysical properties will still be substantially influenced by the length (and/or width) of the aggregates. For a fixed width, properties (such as the J-band width) will change with $1/\sqrt{N}$ where N is the number of monomers." In fact, a very similar sharp emission band has been attributed to such phenomenon before for tetra-(4-sulfonatophenyl)porphyrin (**TPPS**) type molecules [52, 53], as well as other porphyrins [54-56] and **ZnTPP** [57].

**Fluorescence lifetime determination using time-correlated single photon counting (TC-SPC)**

Fig. **7** shows the fits of the $S_1$ decay kinetics of **THOPP** in THF, and in a spin coated thin film at full laser power and half laser power (0.44 mW and 0.22 mW, respectively). The individual $S_1$ decay traces are shown in the supplementary information (Fig. **S11-S13**).

<Fig. **7**>

**THOPP** in solution has a much longer $S_1$ lifetime than in the film, as clearly shown above. (Note that the time axis of **THOPP** in solution has been reduced with a factor 10, for easy comparison of the shapes fo the decay curves). The $S_1$ state in solution decays slower than in the film (Fig. **S11-S13**). Within the film, the laser power does not appear to have much effect on the lifetime (Table **4**). Intuitively, the $\tau_2$ is longer in the half-power data (approx. 0.1 ns longer) as the weaker laser power causes depopulation of the $S_1$ state at a slower rate. In the thin film, the singlet decays *via* bi-exponential decay kinetics in both laser power conditions applied (100% and 50%). Both short lifetimes of **THOPP** at full laser power (0.44 mW) in the film are both enhanced when reducing the laser power to half power (see Table **4**). The shortest lifetime obtained from the bi-exponential fitting is likely due to singlet-singlet annihilation. To our knowledge, these are the first reported fluorescence lifetimes of this particular porphyrin in a solid thin film.

**Porphyrin film: Singlet oxygen detection**

In order to measure the singlet oxygen production of **THOPP** in a solid film, a solvent or medium is needed to detect the singlet oxygen generated. The main reason for this is that the emission intensity of singlet oxygen depends on its steady state concentration present in a particular solvent [58]. The UV-Vis and emission spectra of the films obtained *via* spin coating are conducted in air (Film spectra in Fig. **5** and **6**). Attempts were conducted to measure singlet oxygen emission in air using these films, however there was no signal detected. Moreover, even though the singlet oxygen lifetime is sufficiently long in organic solvents [59], it was found that the porphyrin thin films obtained by spin coating dissolve in organic solvents. Thus, an aqueous solvent, a reliable method to detect singlet oxygen, and films that are stable in aqueous media, were needed. Surprisingly, the spin coated films of **THOPP** were not stable in aqueous media, and peeled of the surface after prolonged (few hours) exposure to water.

A water-soluble chemiluminescent singlet oxygen probe called AquaSpark, that shows an emission maximum at 515 nm upon activation, is an ideal candidate (see mechanism of emission in fig. **S14**) [58]. This probe has been shown to be selective towards singlet oxygen compared to other reactive oxygen species [58]. Films that are stable in aqueous media, and are thus water-resistant, were made using a vapour-phase deposition technique (see experimental section) and its photophysical properties were determined. The UV-Vis spectrum of this PVD film is shown below (Fig. **8**) and the data is summarized in Table **3**.

<Fig. **8**>

The UV-Vis spectrum of the thin film made by vapour-phase deposition shows a profile similar to that observed in solution and in the films made by spin coating (Table **4**; Fig. **8**). The spectrum has the characteristics of a porphyrin: a large Soret band and four small Q-bands. The Q-bands are visible and compared to the spin coated thin film, the Soret band is less intense compared to the Q-bands and all of the peaks appear to be red-shifted by at least 5 nm. This film was excited with 418 nm light and an emission spectrum was recorded (Fig. **9**). Compared to the films made by spin coating, there is no J-band observed in the emission spectrum of these films made by vapour phase deposition (Fig. **9**). Therefore, this is strong evidence that J-aggregates are formed during the spin coating process, but not *via* the vapour-phase deposition technique, nor are they present when **THOPP** is dissolved in $CHCl_3$ or THF (Fig. **S9-S10**). We can use the Full Width at Half Max (FWHM) of the first emission band as a representation of the energetic distribution of the density of states involved in the emissive processes. Using 646 & 657 nm for the spin coated film gives a $\Delta E = 260$ cm$^{-1}$. For the molecules in solution and the PVD film this results in $\Delta E = 575$ cm$^{-1}$ and $\Delta E = 657$ cm$^{-1}$ respectively (using 647 & 672 nm as well as 639 & 667 nm (PVD)). This implies a very narrow energetic distribution for the J-aggregates.

<Fig. **9**>

The **THOPP** thin film was placed in a large cuvette containing the AquaSpark solution and a chemiluminescence emission spectrum with a maximum at ~ 500 nm was obtained upon 650 nm excitation of the porphyrin (Fig. **10**).

<Fig. **10**>

Porphyrin excitation at 650 nm leads to singlet oxygen formation that activates the AquaSpark probe producing 500 nm emission through a chemiluminescent reaction. This shows that the **THOPP** photosensitizer (PS), even in a thin film, is capable of producing singlet oxygen. As reference material a quartz plate was used (no PS present). The excitation wavelength used was 650 nm (red light). This was chosen as the production of singlet oxygen *via* red (or even better, NIR, above 750 nm) light is highly desirable for photo medical applications. The red (or NIR) light can penetrate deep into the human tissue to activate the PS in the thin film. In future developments, this film could than be present on an implant and produce $^1O_2$ for antimicrobial effects.

## CONCLUSION

We present a method to make porphyrin thin films that are stable to aqueous exposure and are able to generate singlet oxygen. Physical Vapour Deposition is needed as, unfortunately, spin coated films do not result in films that are stable to exposure to aqueous media. The PVD films can generate singlet oxygen upon excitation with light, which can be detected by using the chemiluminescent Aqua-spark probe. This is a very sensitive and versatile methodology. The **THOPP** compound was used as the active component in the proof of principle for this method, and it can form suitable films. A novel approach is thus to apply **THOPP** as a photosensitizer in a thin film. As shown in literature, due to its long alkyl tails, the film formation is improved. **THOPP** was synthesized, and its photophysical properties were determined in solution, using **TPP** as a reference. **THOPP** produces a slightly smaller amount of singlet oxygen compared to **TPP** ($\Phi_\Delta = 0.44$ and 0.55 in $CHCl_3$, respectively). The fluorescence emission and lifetimes in the film are shorter than in solution and the fluorescence lifetime of **THOPP** in a film, as well as its singlet oxygen formation, were

determined. Spin coated films of THOPP show a characteristic sharp J-band emission (at 741 nm), indicating well organized J-aggregates.

**Future outlook**

The future potential impact of this work is that a water-resistant porphyrin thin film could be activated using near IR light. The near IR light is known to be able to penetrate deep within human tissue to produce singlet oxygen that can kill cancer or bacteria in the body. In the future, this type of films can be envisaged as a novel way to clean an implant: porphyrin thin films may produce singlet oxygen that could kill bacteria that are accumulating at an implant.

## EXPERIMENTAL

The synthesis was carried out in the laboratories of Porphychem, Dijon, France.

### SYNTHESIS

**THOPP** was synthesized (Fig. **1**) *via* a modified literature procedure (see supplementary information for the characterization data-figs **S1-S6**) [22].

<Fig. **16**>

### SYNTHETIC PROCEDURE

4-Hexyloxybenzaldehyde (5.00 mL, 4.96 g, 24.04 mmol, 1.00 eq.), freshly distilled pyrrole (2.60 mL, 2.51 g, 37.48 mmol, 1.56 eq.) and 1 mL acetic anhydride was dissolved in 100 mL propionic acid. The reaction mixture was stirred under reflux conditions at 130 °C for 4 hours. The reaction mixture was cooled slowly to room temperature. The reaction mixture was then filtered and the filtrate was washed with methanol. The crude product was then recrystallized using a 1 : 1 chloroform : methanol mixture and the product was filtered. The product was washed with methanol and allowed to dry overnight to obtain a shiny crystalline purple solid containing prism shaped crystals. Yield = 1.17 g (12%), mp 274.9–275.6 °C. UV-Vis (THF): $\lambda_{max}$ (log ε) 421 (5.64), 518 (4.13), 552 (3.97), 597 (3.15), 652 (4.13). $^{1}$H NMR (500 MHz; $CDCl_3$): δ, ppm -2.74 (2H, s, NH), 0.99 (12 H, t, $J$ = 7.0 Hz, $CH_3$), 1.46 (16 H, m, $(CH_2)_2$), 1.64 (~8 H, m, γ-$CH_2$ + $H_2O$), 1.99 (8 H, m, β-$CH_2$), 4.26 (8 H, t, $J$ = 7 Hz, α-$CH_2$), 7.27 (8 H, d, $J$ = 9.0 Hz, $H_{ar}$ meta), 8.10 (8 H, d, $J$ = 9.0 Hz, $H_{ar}$ ortho), 8.86 (s, 8 H, pyr-$H_β$) $^{13}$C NMR (600 MHz, $CDCl_3$): δ13.14 ($CH_3$), 22.72 ($CH_2$), 25.94 ($CH_2$), 29.50 ($CH_2$), 31.75 ($CH_2$), 68.35 (α-$CH_2$), 112.71 ($C_{ar}$(meta)), 119.82 ($C_{ar}$(meso)), 131.10 (pyrrole carbons, very broad and weak due to NH exchange), 134.48 ($C_{ar}$(ipso)), 135.61($C_{ar}$(ortho)), 158.98 ($C_{ar}$-O(para)). MS (MALDI): Calcd for $C_{68}H_{78}N_4O_4$: *m/z* 1014.60 ($[M]^+$). Found: *m/z* 1014.53 ($[M]^+$).

### PHOTOPHYSICAL CHARACTERIZATION IN SOLUTION

#### *MATERIALS AND TECHNIQUES*

The photophysical characterization was conducted in $CHCl_3$ and THF (spectroscopy grade, supplier = Merck) in Amsterdam, Netherlands. Melting point was determined with a Reichert melting point microscope equipped with a Pt-100 temperature element. Using this equipment, **TPP** had a melting point of (301.4 -> 302.3 °C)

#### *ABSORPTION AND PHOTOLUMINESCENCE SPECTRA*

Both UV-Vis absorption spectra and fluorescence emission spectra were recorded at 21 °C. UV-Vis absorption spectra were measured in quartz cuvettes (1 cm path-length, Hellma) using a HP/Agilent 8453 UV-Vis and Shimadzu UV2700 spectrophotometer. Fluorescence emission spectra were recorded on a SPEX Fluorolog 3 fluorometer. In this fluorometer, double grating monochromators are used in the excitation and emission channels. A Xenon arc lamp (450 W, Osram) is the excitation light source, and a Peltier cooled photomultiplier tube (R636-10, Hamamatsu) is the detector. The fluorescence signal from the fluorophores in solution is collected in a right-angle geometry, and the fluorescence spectra are corrected for fluctuations of the excitation source flux and for the wavelength dependence of the detection sensitivity. The absorbance for photoluminescence spectra was approximately 0.1 for solution.

***FLUORESCENCE AND SINGLET OXYGEN QUANTUM YIELDS***

Both quantum yields were determined using the SPEX fluorolog 3 fluorometer relative to a fluorescent/singlet oxygen standard of a known quantum yield. From here, the integrated emission spectra of the unknown sample are compared with that of the standard under the same absorbance conditions (absorbance = 0.1) at the same excitation wavelength. The integrated emission spectra are corrected for the skewed baselines where appropriate.

For these measurements, dilute solutions with absorbances of approximately 0.1 at one of the Q-bands in the absorption spectrum were used. Absorption and emission spectra (both fluorescence and singlet oxygen) were measured using 3.0 ml of the sample and standard solutions in 1 x 1 cm optical path length quartz cells. The quantum yields were calculated using the equation **4** below [60]:

$$Q_x = Q_r[A_r(\lambda_r)/A_x(\lambda_x)][I(\lambda_r)/I(\lambda_x)][(n_x)^2/(n_r)^2](D_x/D_r) \quad \text{(Equation 4)}$$

Where $Q_x$ = the desired quantum yield (fluorescence or singlet oxygen) of the unknown sample; $Q_r$ = the (fluorescence of singlet oxygen) quantum yield of the known sample according to literature; $A_r(\lambda_r)$ = absorbance of the reference at the excitation wavelength; $A_x(\lambda_x)$ = absorbance of the unknown sample at the excitation wavelength; $I(\lambda_r)$ = relative intensity of the exciting light of a known reference at wavelength λ; $I(\lambda_x)$ = relative intensity of the exciting light of an unknown sample at wavelength λ; $n_x$ = refractive index of the solvent that the unknown sample is dissolved in; $n_r$ = refractive index of the solvent that the known sample is dissolved in; $D_x$ = integrated area under the corrected emission spectrum of the unknown sample; $D_r$ = integrated area under the corrected emission spectrum of the known sample. In both cases, the integrated area was corrected for the skewed baseline (if present), thereby lowering the area under the emission curve. The data was analyzed using the Origin program and excel [61]. **Note:** For singlet oxygen measurements, the unknown and reference sample were in the same solvent.

***NANOSECOND TRANSIENT ABSORPTION SPECTRA***

Triplet state lifetimes were determined by means of nanosecond time-resolved absorption spectroscopy using an EKSPLA NT342B laser system in which the third harmonic of a Nd:YAG laser system (355 nm) was used to pump an OPO (to give $\lambda_{ex}$ = 517 nm, pulse width which has an adjustable gate width of minimal 2.9 ns and laser power range of 1–3 mJ per pulse). This setup is described in full detail in the literature [62]. The data was analyzed using Igor 7 Pro (Wavemetrics, Lake Oswego, OR, USA) [63]. The absorbances of the solutions used were approximately 0.5. For the oxygen-free solution, the solution was bubbled with argon for 1–2 hours prior to laser excitation *via* this setup.

***TIME CORRELATED SINGLE PHOTON COUNTING SPECTRA***

Time-resolved emission measurements were performed on a picosecond single photon counting setup. The excitation wavelength (560 nm) is generated by the output of a fully automatic tunable Ti:sapphire laser (Chameleon Ultra, Coherent). This source produces a sub-picosecond excitation pulse, (full-width half-maximum, FWHM). The repetition rate is decreased from the fundamental 80 MHz to a lower value (usually 8 MHz) using a pulse picker (Pulse Select, APE). After second harmonic generation (SHG), a dichroic mirror is used to separate the doubled light which is directed to the sample. Fundamental light is guided *via* a delay line to a fast photodiode (PD) and used as a reference pulse. The emission is collected at a 'magic angle' (54.7 °) and focused onto a multichannel plate photomultiplier tube (MCP-PMT,

R3809U-50, Hamamatsu) through a single-grating monochromator (Newport Cornerstone 260, f=250mm, grating 300ln/mm blaze 422 or grating 300ln/m blaze 750nmM20, Carl Zeiss, 600 lines/mm). Although the excitation source produces sub-picosecond pulses, the electronics and the detector cause a broadening of the signal and are the limiting factor of the time resolution. The overall instrument response function (IRF) was 20 ps (FWHM) for the solution of the measured compound, which is measured from a dilute scattering solution (Ludox) at the excitation wavelength.

**SOLID THIN FILMS**

***PRECLEANING***

Three square quartz glass slides (see provider and description below) were washed with a brush, soap and water in a beaker. The slides were then placed into a Teflon substrate holder using forceps. The glass slides in the substrate holder were submerged in deionized water before sonication for 15 minutes. The water was then replaced by acetone and the beaker was further sonicated for 15 minutes. The acetone was replaced by isopropanol and further sonicated for 15 minutes. The glass slides were allowed to dry. Compressed air was used to accelerate the drying process. The glass slides were then placed back into the substrate holder and were placed inside a UV-ozone photoreactor for 30 minutes.

***PROVIDER AND DESCRIPTION OF THIN FILMS***

**Provider of thin film substrates:** Präzisions Glas & Optik GmbH;

**Description:** 2.5 x 2.5 $cm^2$ quartz glass substrates with a thickness of 1.1 mm-CNC precision-cut, no bevel.

***SPIN COATING PROCEDURE FOR THIN FILM FORMATION***

Three quartz glass slides were cleaned with the precleaning technique as described above. Directly after being removed from the UV-ozone photoreactor, the slides were mounted on the spin coating machine (Delta 10, Ble Laboratory Equipment GmbH). The vacuum was switched on to approximately 0.6 bar for fixation. The spin speed (2000 rpm), spinning time (30 s) and acceleration (9 = slowest acceleration) were set.

10 mg/ml **THOPP** in THF solvent were prepared, sonicated and filtered (PVDF filter, 0.45 µm) into a sample vial. 0.3 ml was deposited on the glass, giving full coverage. Spinning was started. After spin coating the films were allowed to dry for 24 hours under ambient conditions in the dark. $CHCl_3$ can also be used as a solvent, but THF is better suited as it less volatile. 10 mg/ml was used as such a highly concentrated solution is needed for spin coating and in most cases gives good results.

***VAPOUR-PHASE DEPOSITION PROCEDURE FOR THIN FILM FORMATION***

Three glass slides were cleaned with the precleaning technique as described above. Almost immediately after being removed from the UV-ozone photoreactor, 10 mg of the **THOPP** porphyrin was then placed at the bottom of a 100 ml two-neck round bottom flask. A slide was then carefully placed to be over the porphyrin solid. The flask was carefully attached to a Schlenk line and the pressure of the system inside the flask was reduced to $10^{-4}$ mbar. The solid was then heated slowly from 250 $^oC$ to 400 $^oC$ using a heat gun or until the solid had been vaporized and formed a layer on the slide. The slide was then allowed to cool to room temperature to create a water stable thin film.

***ABSORPTION AND PHOTOLUMINESCENCE SPECTRA OF THIN FILMS***

Both UV-Vis absorption spectra and fluorescence emission spectra were recorded at 21 $^oC$ and on a thin film support. The instruments were then used as described above for the solution.

### *TIME CORRELATED SINGLE PHOTON COUNTING OF A THIN FILM*

The time-resolved emission measurements were performed as described above for the solution. The differences were that the film was placed on a thin film support and the overall instrument response function (IRF) was 8 ps (FWHM) for the thin film.

### *AQUASPARK™ 515 SINGLET OXYGEN PROBE*

This singlet oxygen probe was obtained from Carbosynth and a 50 ml 2 μM AquaSpark PBS solution was made. For measuring singlet oxygen, the excitation wavelength used was 650 nm and emission was observed from 450 nm to 550 nm, using the same settings as the fluorescence emission spectra. The film was placed into a large cuvette (20 ml capacity) and the **THOPP** film was excited in the presence of the AquaSpark probe. A quartz slide was used as a reference.

## ACKNOWLEDGEMENTS

This project has received funding from the European Union's Horizon 2020 research and innovation programme under the Marie Sklodowska-Curie grant agreement no. 764837.

## SUPPORTING INFORMATION

The synthetic characterization, spectra and extra photophysical data are given in the supplementary material.
In relation to Research Data Management, this data is also available here:
https://doi.org/10.21942/uva.18865448

## REFERENCES

1. Callaghan S and Senge MO. *Photochem. Photobiol. Sci.* 2018; **17**: 1490-1514.
2. Finsen NR. La Photothérapie, Georges Carré et C. Naud, Paris, 1899.
3. Agostinis P, Berg K, Cengel KA, Foster TH, Girotti AW, Gollnick SO, Hahn SM, Hamblin MR, Juzeniene A, Kessel D, Korbelik M, Moan J, Mroz P, Nowis D, Piette J, Wilson BC and Golab J. *CA Cancer J. Clin*. 2011; **61**: 250-281.
4. Kalka K, Merk H and Mukhtar H. *J. Am. Acad. Dermatol*. 2000; **42**: 389-413.
5. Wainwright M. *Photochem. Photobiol. Sci*. 2019; **18**: 12-14.
6. De Silva P, Saad MA, Thomsen HC, Bano S, Ashraf S and Hasan T. *J. Porphyrins Phthalocyanines*. 2020; **24**: 1320-1360.
7. Gunaydin G, Emre Gedik M and Ayan S. *Front. Chem.* 2021; **9**: 691667.
8. Abrahamse H and Hamblin MR. *Biochem. J*. 2016; **473**: 347-364.
9. Chen Q, Dan H, Tang F, Wang J, Li X, Cheng J, Zhao H and Zeng X. *Int. J. Oral Sci.* 2019; **11**: 1-5.
10. Zhao J, Wu W, Sun J and Guo S. *Chem. Soc. Rev.* 2013; **42:** 5323-5351.
11. Calixto GMF, Bernegossi J, de Freitas LM, Fontana CR and Chorilli M. *Molecules*. 2016; **21**: 342-359.
12. Gibbons DJ, Farawar A, Mazzella P, Leroy-Lhez S and Williams RM. *Photochem. Photobiol. Sci.* 2020; **19**: 136-158.
13. Nguyen V-N, Yan Y, Zhao J and Yoon J. *Acc. Chem. Res*. 2021; **54**: 207-220.
14. Dąbrowski JM, Pucelik B, Regiel-Futyra A, Brindell M, Mazuryk O, Kyzioł A, Stochel G, Macyk W and Arnaut LG. *Coord. Chem. Rev*. 2016; **325**: 67-101.

15. Cieplik F, Deng D, Crielaard W, Buchalla W, Hellwig E, Al-Ahmad A and Maisch T. *Crit. Rev. Microbiol.* 2018; **44**: 571-589.
16. Wainwright M. *Dyes Pigm.* 2017; **146**: 402-407.
17. Gursoy H, Ozcakir-Tomruk C, Tanalp J and Yilmaz S. *Clin. Oral Investig.* 2013; **17**: 1113-1125.
18. Ambrosini V, Issawi M, Sol V, Riou C. *Sci. Rep.* 2020; **10**: 17438.
19. Utari AW, Purnama B and Abraha K. *Adv. Mater. Res.* 2014; **896**: 187-191.
20. Long B, Bakr O and Stellacci F. *J. Exp. Nanosci.* 2008; **3**: 53-60.
21. Shimizu Y, Miya M, Nagata A, Ohta K, Yamamoto I and Kusabayashi S. *Liq. Cryst*. 1993; **14**: 795-805.
22. Charisiadis A, Bagaki A, Fresta E, Weber KT, Charalambidis G, Stangel C, Hatzidimitriou AG, Angaridis PA, Coutsolelos AG and Costa RD. *ChemPlusChem*. 2017; **82**: 1-13.
23. Zielenkiewicz W, Perlovich GL, Nikitina GE and Golubchikov OA. *J. Solution Chem.* 1997; **26**: 663-679.
24. Topal SZ, Ongun MZ, Önal E, Ertekin K and Hirel C. *Dyes and Pigments*. 2017; **144**: 102-109.
25. Şen P, Hirel C, Andraud C, Aronica C, Bretonnière Y, Mohammed A, Ågren H, Minaev B, Minaeva V, Baryshnikov G, Lee HH, Duboisset J and Lindgren M. *Materials*. 2010; **3**: 4446-4475.
26. Bhyrappa P, Arunkumara C, Varghesea B, Rao DSS and Prasad SK. *J. Porphyrins Phthalocyanines*. 2008; **12**: 54-64.
27. Minamijima N, Furuta N, Wakunami S and Mizutani T. *Bull. Chem. Soc. Jpn*. 2011; **84**: 794-801.
28. Adler AD, Longo FR, Finarelli JD, Goldmacher J, Assour J and Korsakoff L. *J. Org. Chem.* 1967; **32**: 476-476.
29. Abraham RJ, Hawkes GE, Hudson MF and KM Smith. *J. Chem. Soc., Perkin trans. 2*. 1975; **3**: 204-211.
30. Green MK, Medforth CJ, Muzzi CM, Nurco DJ, Shea KM, Smith KM, Lebrilla CB and Shelnutt JA. *Eur. Mass Spectrom.* 1997; **3**: 439-451.
31. Antolovich M, Nguyen TH, Paddon-Row MN and Willett GD. *Org. Mass Spectrom*. 1992; **27**: 1034-1041.
32. Castro AJ, Van Berkel GJ, Dolittle FG and Filby RH, *Org. Geochem*. 1989; **14**; 193-202.
33. Woods JS and Simmonds PL. *Curr Protoc Toxicol*. 2001; **7**: 8.9.1-8.9.17.
34. Sun Z-C, She Y-B, Zhou Y, Song X-F and Li K. *Molecules*. 2011; **16**: 2960-2970.
35. Bruhn T and Brückner C. *Phys. Chem. Chem. Phys.* 2015; **17**: 3560-3569.
36. Seybold PG and Gouterman M. *J. Mol. Spectrosc*. 1969; **31**: 1-13.
37. Zakavi S and Hoseini S. *RSC Advances*. 2015; **5**: 106774-106786.
38. Eom I and Joo TJ. *Chem. Phys*. 2009; **131**: 244507.
39. Montalti M, Credi A, Prodi L and Gandolfi MT. Handbook of Photochemistry, CRC Press, 2006.
40. Mazur LM, Roland T, Leroy-Lhez S, Sol V, Samoc M, Samuel IDW and Matczyszyn K. *J. Phys. Chem*. 2019; **123**: 4271-4277.
41. Röder B, Büchner M, Rückmann I and Senge MO. *Photochem. Photobiol. Sci*. 2010; **9**: 1152-1158.
42. Singh-Rachford TN and Castellano FN. *Coord. Chem. Rev*. 2010; **254**: 2560-2573.
43. Wang Z, Ivanov M, Gao Y, Bussotti L, Foggi P, Zhang H, Russo N, Dick B, Zhao J, Di Donato M, Mazzone G, Luo L and Fedin M. *Chem. – Eur. J*. 2020; **26**: 1091-1102.
44. Ebbesen TW, Tanigaki K and Kuroshima S. *Chem. Phys. Lett.* 1991; **181**: 501-504.
45. Sagadevan A, Hwang KC and Su MD. *Nat. Commun.* 2017; **8**: 1-8.
46. Magna G, Monti D, Di Natale C, Paolesse R and Stefanelli M. *Molecules*. 2019; **24**: 4307-4338.
47. Gouterman M. *J. Mol. Spectrosc.* 1961; **6**: 138-163.
48. Kasha M, In Spectroscopy of the Excited State.; Di Bartolo, B., Ed.; Plenum Press: New York, 1975, p 340.
49. Dong B, Galka CH, Gade LH, Chi L and Williams RM. *Nanopages*. 2006; **3**: 325-338.

50. Würthner F, Kaiser TE and Saha-Möller CR. *Angew. Chem. Int. Ed*. 2011; **50**: 3376-3410.
51. Keller N, Calik M, Sharapa D, Soni HR, Zehetmaier PM, Rager S, Auras F, Jakowetz AC, Görling A, Clark T and Bein T. *J. Am. Chem. Soc.* 2018; **140**: 16544-16552.
52. Venkatramaiah N, Ramakrishna B, Venkatesan R, Almeida Paz FR and Tomé JPC. *New J. Chem.* 2013; **37**: 3745-3754.
53. Liu LL, Zhao YF and Jin WJ. *J. Porphyr. Phthalocyanines*. 2012; **16**: 1132-1139.
54. Jellen CP and Bettermann H. S*pectrochim. Acta. A. Mol. Biomol. Spectrosc*. 2003; **59**: 463-470.
55. Ma H, Sun S, Chen X, Wu D, Zhu P, Du B and Wei Q. *J. Porphyr. Phthalocyanines*. 2008; **12**: 101-108.
56. Han Q, Wang C, Li Z, Wu J, Liu PK, Mo F and Fu Y. *Anal. Chem*. 2020; **92**: 3324-3331.
57. Zakharova IB, Elistratova MA, Romanov NM and Kvyatkovskii OE. *Semiconductors*. 2018; **52**: 1708-1714.
58. Hananya N, Green O, Blau R, Satchi-Fainaro R and Shabat D. *Angew. Chem. Int. Ed.* 2017; **56**: 11793-11796.
59. Wilkinson F, Helman WP and Ross AB. *J. Phys. Chem. Ref. Data*. 1995; **24**: 663-677.
60. Demas JN and Crosby GA. *Am. J. Phys. Chem.* 1971; **75**: 991-1024.
61. Origin, Version 2018b. OriginLab Corporation, Northampton, MA, USA.
62. Kumpulainen T, Bakker BH, Hilbers M and Brouwer AM. *J. Phys. Chem. B*. 2015; **119**: 2515-2524.
63. Igor Pro (Wavemetrics, Lake Oswego, OR, USA).

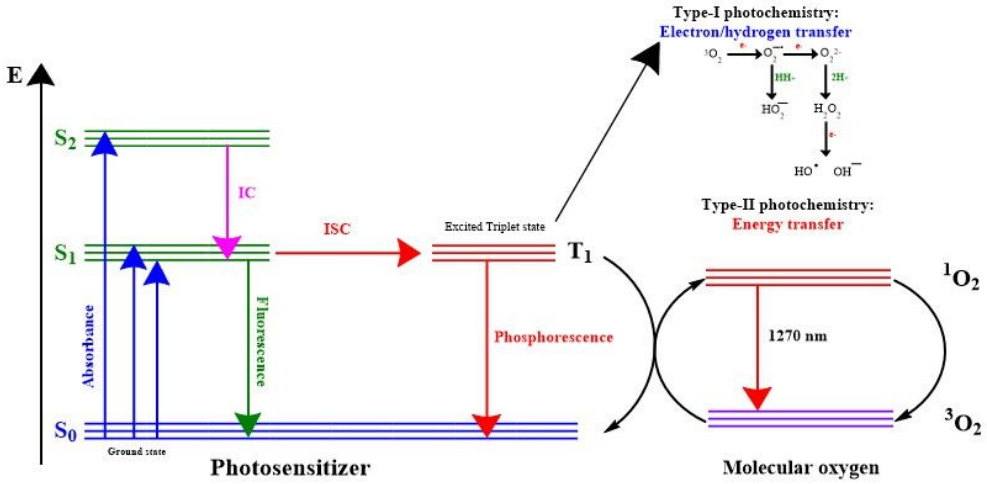


**Fig. 1.** Jablonski energy diagram showing how the photosensitizer is excited to the singlet state ($S_1$), followed by population of the excited triplet state by intersystem crossing (ISC) and the triplet state interacting with molecular oxygen to form reactive oxygen species and cytotoxic singlet oxygen [14]. IC represents isoenergetic internal conversion (from $S_2$ to higher vibrational states of $S_1$) followed by downhill vibrational relaxation.

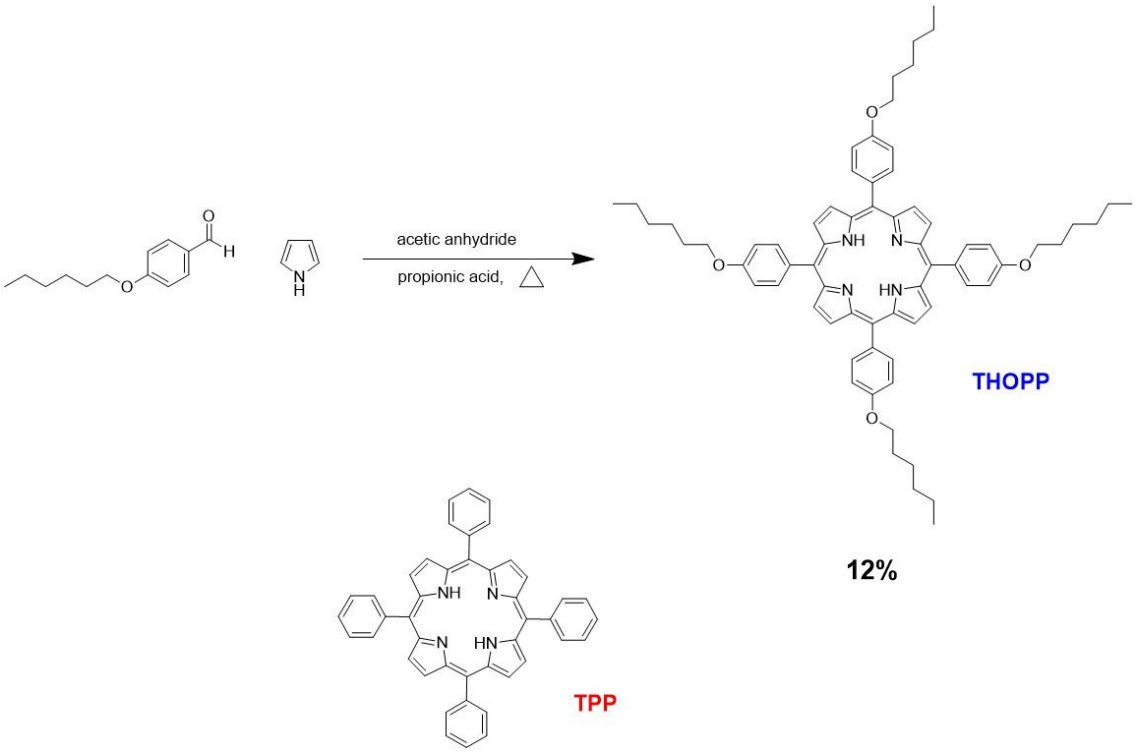


**Fig. 2. (Top):** Reaction scheme for the synthesis of 5,10,15,20 -tetra -4 -hexyloxyphenylporphyrin (**THOPP**) and **(Bottom):** chemical structure of 5,10,15,20 -tetraphenylporphyrin (**TPP**) [22].

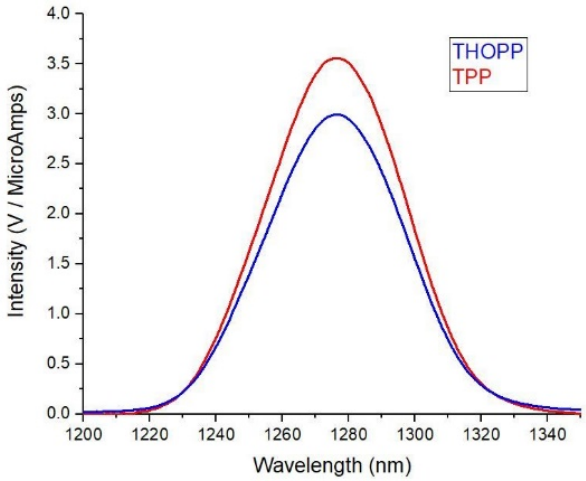


**Fig. 3.** Singlet oxygen emission induced by **THOPP** (blue) and **TPP** (red) in $CHCl_3$ using **TPP** in $CHCl_3$ as a reference (0.55) [40]. Excitation wavelength = 521 nm and the obtained singlet oxygen quantum yield was 0.44.

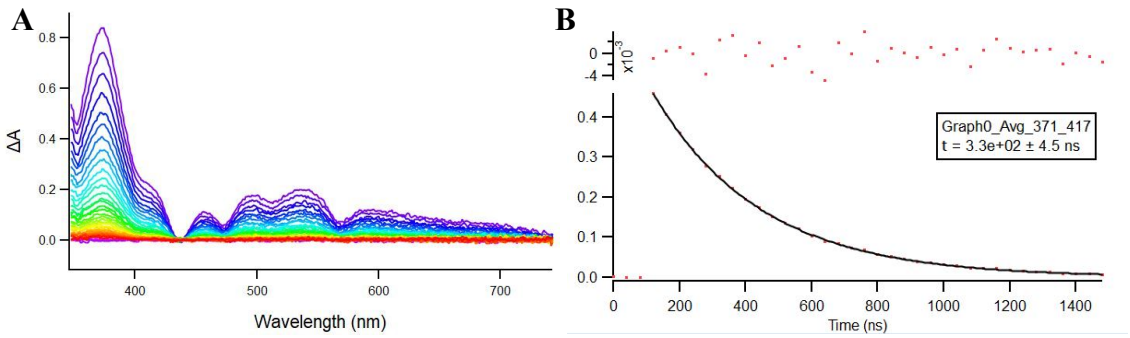


**Fig. 4.** (**A**): Nanosecond transient absorption spectrum of **THOPP** in THF (in air). $\lambda_{ex}$ = 518 nm, incremental time delay = 40 ns, time increasing from purple to red. (**B**): Decay kinetics trace at 517 nm. Decay curve is fitted mono -exponentially and the obtained triplet lifetime is 330 ns. On the top, weighted residuals are presented.

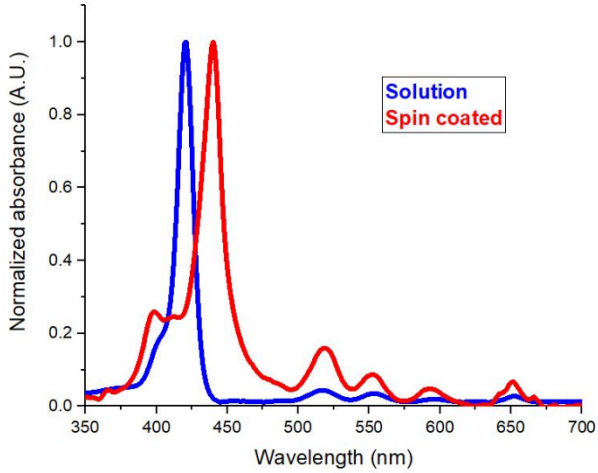


**Fig. 5.** Overlapped and normalized UV-Vis spectrum of **THOPP** in THF solution (**blue**) and in a thin film spin coated onto quartz glass (**red**).

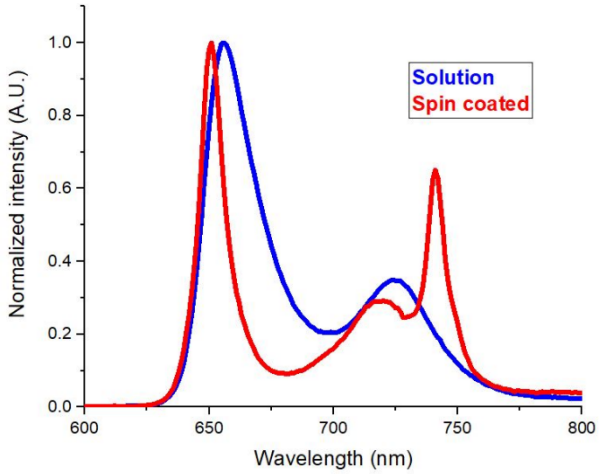


**Fig. 6.** Overlapped normalized emission spectrum of spin coated **THOPP** thin film on quartz glass (**red**) and **THOPP** in $CHCl_3$ solution (**blue**). Excitation wavelength= 440 nm.

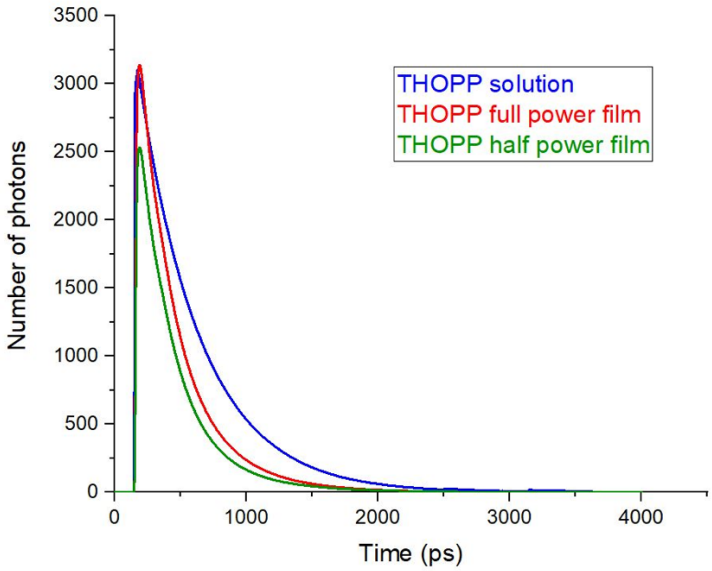


**Fig. 7.** Overlapped Time -correlated single photon counting (TC -SPC) fitted data of **THOPP** in THF solution (blue) and a thin film, at a full laser power (red) and half laser power (green). Excitation wavelength = 560 nm. Emission wavelength = 650 nm. The absorbance was 0.05 at the excitation wavelength for all species. Full power includes the laser power being at 0.44 mW while at half power, the laser power is 0.22 mW. The time axis of **THOPP** in solution has been divided by a factor 10.

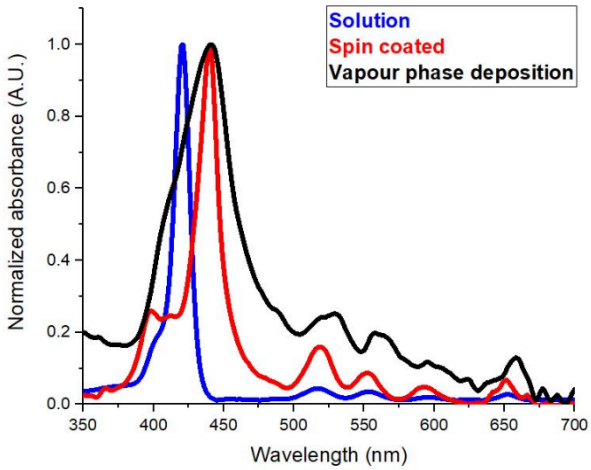


**Fig. 8.** Overlapped normalized UV-Vis spectrum of **THOPP** dissolved in THF solvent (**blue**), in a thin film on quartz glass obtained by spin coating (**red**) and in a thin film on quartz glass made by vapour -phase deposition (**black**).

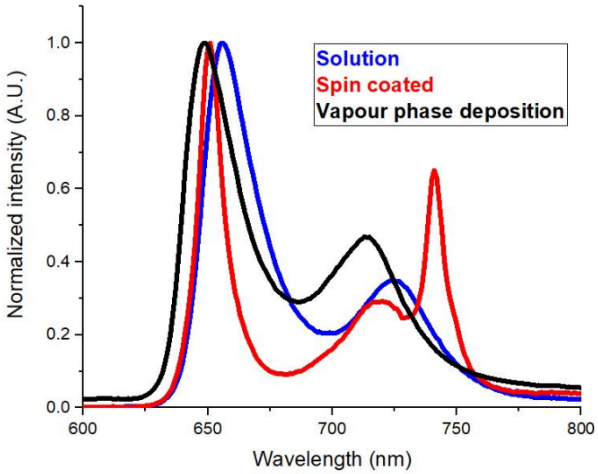


**Fig. 9.** Overlapped normalized fluorescence emission spectrum of **THOPP** dissolved in $CHCl_3$ solvent (**blue**), **THOPP** in a thin film on quartz glass obtained by spin coating (**red**), and **THOPP** in a thin film on quartz glass made by vapour -phase deposition (**black**).

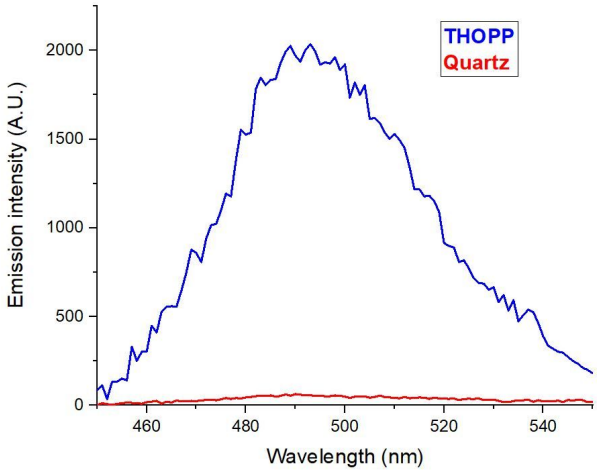


**Fig. 10.** Singlet oxygen detection via chemiluminescence of the AquaSpark probe after selective excitation of the **THOPP** PS in a PVD thin film. The reference is a quartz plate in AquaSpark probe solution. Excitation wavelength = 650 nm.

Table **1**. UV-Vis absorption data of the PSs, **THOPP** and **TPP**. The concentration was 2.3 μM for **THOPP** in $CHCl_3$, 2.2 μM for **THOPP** in THF, and 1.6 μM for **TPP** in $CHCl_3$. Values in brackets refer to the log of the molar absorption coefficient (ε).

| **PS** | **Sh** [a] **(λ/nm)** | **Soret band (λ/nm)** | **Q -bands (λ/nm)** | | | | **$Q_{III}$ / Soret** [b] |
|---|---|---|---|---|---|---|---|
| | | | **$Q_{IV}$** [c] | **$Q_{III}$** [d] | **$Q_{II}$** [e] | **$Q_I$** [f] | |
| **THOPP – $CHCl_3$** | 400 | 423 (5.65) | 521 (4.40) | 556 (4.32) | 594 (4.14) | 655 (4.20) | 0.02 |
| **THOPP -THF** | 400 | 421 (5.64) | 518 (4.16) | 554 (4.02) | 596 (3.56) | 654 (3.84) | 0.02 |
| **TPP – $CHCl_3$** | 400 | 418 (5.76) | 515 (4.35) | 550 (3.97) | 590 (3.82) | 644 (3.69) | 0.02 |

[a] Sh = shoulder that appears beside Soret band; [b] Ratio of the intensity of the $Q_{III}$ band compared to the Soret band; [c] $Q_{IV}$ = Qy(1,0) peak; [d] $Q_{III}$ = Qy(0,0) peak; [e] $Q_{II}$ = Qx(1,0) peak; [f] $Q_I$ = Qx(0,0) peak.

Table **2**. Photophysical properties of **THOPP** in THF and $CHCl_3$, and **TPP** in $CHCl_3$.

| PS | Em1 [a] (nm) | Em2 [a] (nm) | SS [b] ($cm^{-1}$) | $\Phi_f$ [c] | $\Phi_\Delta$ [d] | $\tau_s$ (ns) [e] | $\tau_T$ (ns) [f] | $\tau_T$ (µs) [g] | |
|---|---|---|---|---|---|---|---|---|---|
| | | | | | | | | $\tau_1$ | $\tau_2$ |
| **THOPP – $CHCl_3$** [h] | 655 | 725 | 70 | 0.22 | 0.44 | -[i] | -[i] | -[i] | -[i] |
| **THOPP – THF** [j] | 655 | 725 | 70 | 0.22 | -[i] | 9.4 ± 0.9 | 330 ± 4.5 | 297 | 46 |
| **TPP – $CHCl_3$** [h] | 649 [h] | 718 [h] | 120 [h] | 0.11 [h] | 0.55 [h] | 10.6 ± 0.3 [k] | 480 [k] | 385 [k] | * |

[a] According to the emission spectra, Em1 = first emission peak [$\lambda_{em}$ $Q_x(0,0)$] and Em2 = second emission peak [$\lambda_{em}$ $Q_x(0,1)$]; [b] The Stokes shift (SS) that was calculated from the corresponding UV-Vis and emission spectra; [c] $\Phi_f$ = fluorescence quantum yield calculated using TPP (0.11) as a reference in toluene [36]; [d] $\Phi_\Delta$ = singlet oxygen quantum yield was calculated using TPP (0.55) as a reference in $CHCl_3$ [40]; [e] $\tau_s$ = singlet state lifetime in air (equilibrated), given in nanoseconds; [f] $\tau_T$ (ns) = triplet state lifetime in air (equilibrated), given in nanoseconds; [g] $\tau_T$ (µs) = triplet state lifetime in oxygen -free solution (given in microseconds), the triplet state lifetime in the oxygen -free solution undergoes bi -exponential decay giving two lifetimes, $\tau 1$ and $\tau 2$, given in microseconds; [h] in $CHCl_3$ solvent; [i] data not available; [j] in THF solvent; [k] literature values in DMF solvent [41]; * no second lifetime reported in literature, it decays mono -exponentially, thus yielding only one triplet lifetime.

Table **3**. UV-Vis absorption data of **THOPP** in thin films, obtained via spin coating (SC) or by vapour deposition (PVD).

| **PS film** | **Soret band (λ/nm)** | **Sh [a] (λ/nm)** | **Q -bands (λ/nm)** | | | | **$Q_{III}$ / Soret [b]** |
|---|---|---|---|---|---|---|---|
| | | | **$Q_{IV}$ [c]** | **$Q_{III}$ [d]** | **$Q_{II}$ [e]** | **$Q_{I}$ [f]** | |
| **THOPP (SC)** | 440 | 400 | 519 | 551 | 591 | 651 | 0.12 |
| **THOPP (PVD)** | 440 | 400 | 528 | 556 | 601 | 661 | 0.15 |

[a] Sh = shoulder that appears beside Soret band; [b] ratio of the intensities of the $Q_{III}$ and Soret band of the porphyrin in the film; [c] $Q_{IV} = Q_y(1,0)$ peak; [d] $Q_{III} = Q_y(0,0)$ peak; [e] $Q_{II} = Q_x(1,0)$ peak; [f] $Q_I = Q_x(0,0)$ peak.

Table **4**. Photophysical properties of **THOPP** thin films obtained by spin coating (SC) and vapour -phase deposition (PVD).

| **PS** | **Em1** [a] **(nm)** | **Em2** [a] **(nm)** | **Em3** [b] **(nm)** | **$S_1$ lifetime (ns)** [d] | | | |
|---|---|---|---|---|---|---|---|
| | | | | **Full power** [e] | | **Half power** [e] | |
| | | | | **$\tau_1$ (Amp)** [f] | **$\tau_2$ (Amp)** [f] | **$\tau_1$ (Amp)** [f] | **$\tau_2$ (Amp)** [f] |
| **THOPP SC** | 651 | 719 | 741 | 0.745 (0.51) | 0.239 (0.49) | 0.749 (0.42) | 0.368 (0.58) |
| **THOPP PVD** | 648 | 714 | -[g] | -[h] | -[h] | -[h] | -[h] |

[a] According to the emission spectra, Em1 = first emission peak [$\lambda_{em}$ $Q_x(0,0)$] and Em2 = second emission peak [$\lambda_{em}$ $Q_x(0,1)$], Excitation wavelength = 440 nm and emission was measured in nm; [b] Em3 = peak that appears at 741 nm that is due to the formation of a J -aggregate in the film, see fig. **6**; [d] The film of **THOPP** undergoes a bi -exponential decay at both full and half power, due to singlet -singlet annihilation, see fig. **7**; [e] The laser power was changed from full power to half power and it was measured as 0.44 mW and 0.22 mW, respectively; [f] Amp. = amplitude associated with values for bi -exponential fitting. [g] No J-aggregate emission observed in **THOPP** films made with physical vapour-phase deposition (PVD), excitation at 418 nm; [h] No data available.